The influence of vehicle direction of motion in response amplification at railway transition zones

Fărăgău, Andrei B.; Jain, Avni; Metrikine, Andrei V.; van Dalen, Karel N.

DOI
10.1061/9780784485941.022

Publication date
2025

Document Version
Final published version

Published in
ICRT 2024 - Proceedings of the 3rd International Conference on Rail Transportation

The Influence of Vehicle Direction of Motion in Response Amplification at Railway Transition Zones

Andrei B. Fărăgău[1]; Avni Jain[2]; Andrei V. Metrikine[3]; and Karel N. van Dalen[4]

[1]Faculty of Civil Engineering and Geosciences, Delft Univ. of Technology, Netherlands. Email: A.B.Faragau@tudelft.nl
[2]Faculty of Civil Engineering and Geosciences, Delft Univ. of Technology, Netherlands
[3]Faculty of Civil Engineering and Geosciences, Delft Univ. of Technology, Netherlands
[4]Faculty of Civil Engineering and Geosciences, Delft Univ. of Technology, Netherlands

ABSTRACT

Transition zones, characterized by significant variation in track properties (e.g., foundation stiffness) near rigid structures like bridges and tunnels, necessitate more frequent maintenance compared to standard track sections due to higher levels of differential settlements observed at transition zones. Field measurements on one-way tracks reveal asymmetric settlement patterns (i.e., different settlement in the soft-to-stiff vs. stiff-to-soft transitions), yet existing literature often investigate either one or the other transition type without investigating the potential limited validity of results. This study investigates the similar aspects as well as the dissimilar ones regarding the behaviour of soft-to-stiff and stiff-to-soft transitions. Modelling results show that the behaviour of the two transitions can be considerably different. These results strongly suggest that for a mitigation measure to be efficient, it may be necessary to have different designs for the two types of transition wherever possible (i.e., in one-way tracks). This study can help researchers and engineers understand the different degradation patterns obtained using more complex models or from field measurements.

INTRODUCTION

The increased demand on railway transport causes an acceleration in infrastructure degradation leading to an increased frequency of maintenance and repair operations. Transition zones, areas with substantial variation of track properties (e.g., foundation stiffness) encountered near rigid structures such as bridges, tunnels, etc. require considerably more frequent maintenance than the regular parts of the railway track [1]. This is caused by excessive differential settlements that can be related to stresses amplification encountered at transition zones [2–13]. For example, Nielsen et al. [14] found a strong correlation between the track stiffness inhomogeneity and local irregularities in the vertical track geometry (i.e., differential settlement).

Field measurements (e.g., [15]) and numerical simulations (e.g., [16]) on one-way tracks reveal a strongly asymmetric settlement pattern in the soft-to-stiff vs stiff-to-soft transitions. Despite this, the majority of literature studies of transition zones and corresponding countermeasures consider either one or the other transition type without investigating if the results are valid for both transition types. Furthermore, a limited amount of studies (e.g., [17–19]) that treat the difference between these two transition types are available in literature. However, these limited studies focus only on quantitative analysis of the response and its

variation as changes are made to the structure. Currently, there is no clear explanation as to why and under which conditions the response amplification is different for the two transition types.

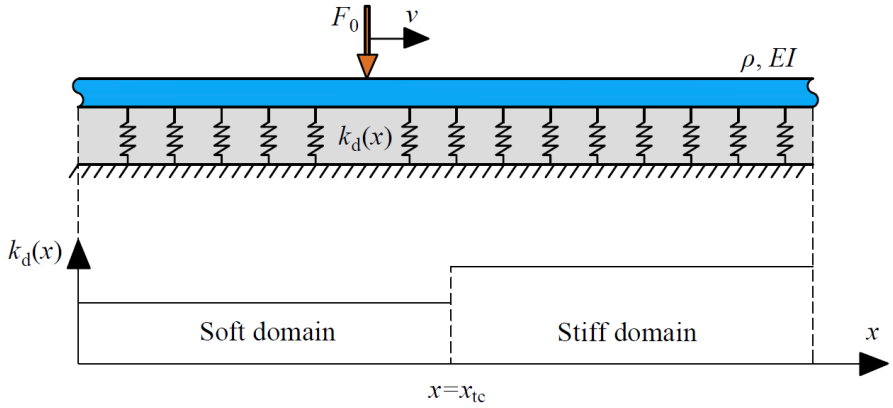

Figure 1: Model schematics: infinite Euler–Bernoulli beam resting on a piecewise-homogeneous Winkler foundation, subject to a moving constant load.

To this end, this study aims to explain and reveal similarities and dissimilarities in behaviour of the (i) soft-to-stiff and (ii) stiff-to-soft transitions. This study is based on work presented by the first author's PhD dissertation [20]. This study can help researchers and engineers understand the different degradation patterns obtained using more complex models or from field measurements.

MODEL FORMULATION AND SOLUTION

To investigate the responses in the soft-to-stiff and stiff-to-soft transitions, we choose one of the simplest representations of a railway track, namely an infinite Euler-Bernoulli beam resting on Winkler foundation acted upon by a moving constant load (Fig. 1). The Winkler foundation has a jump in stiffness at $x = x_{tc}$(subscript tc stands for transition centre), dividing the infinite inhomogeneous domain into two semi-infinite homogeneous ones. The equation of motion of the system reads

$$EIw'''' + \rho\ddot{w} + k_{\mathrm{d}}(x)w = -F_0\,\delta(x - vt), \qquad \forall x, \forall t, \tag{1}$$

$$w(x,t) = \begin{cases} w_{\mathrm{l}}(x,t), & x \le x_{\mathrm{tc}}, \\ w_{\mathrm{r}}(x,t), & x \ge x_{\mathrm{tc}}, \end{cases} \qquad k_{\mathrm{d}}(x) = \begin{cases} k_{\mathrm{d,l}}, & x < x_{\mathrm{tc}}, \\ k_{\mathrm{d,r}}, & x \ge x_{\mathrm{tc}}, \end{cases}$$

where the primes and overdots represent partial derivatives with respect to space and time, respectively, EI and ρ are the bending stiffness and mass per unit length of the beam, respectively, while $k_{d,l}$ and $k_{d,r}$ are the (homogeneous) foundation stiffnesses of the left and right semi-infinite domains, respectively. F_0 and v are the magnitude and the velocity of the moving load, while w_l and w_r represent the displacements of the left and right semi-infinite domains, respectively. The space and time dependency of the unknown displacements is omitted from most expressions for brevity. Furthermore, the use of both the $\leq$ and $\geq$ signs in the definition of $w(x,t)$ emphasizes that there is continuity in this quantity at the interface between the two domains (see below).

At the interface between the two domains, continuity in displacement and slope as well as in shear force and bending moment is imposed. Furthermore, the displacements at infinite distance from the moving load should not be infinite (if material damping is neglected) or should be zero (if material damping is accounted for). The interface and boundary conditions thus read

$$w_\mathrm{l}(x_\mathrm{tc},t) = w_\mathrm{r}(x_\mathrm{tc},t), \qquad w_\mathrm{l}'(x_\mathrm{tc},t) = w_\mathrm{r}'(x_\mathrm{tc},t), \tag{2}$$

$$w_\mathrm{l}''(x_\mathrm{tc},t) = w_\mathrm{r}''(x_\mathrm{tc},t), \qquad w_\mathrm{l}'''(x_\mathrm{tc},t) = w_\mathrm{r}'''(x_\mathrm{tc},t), \tag{3}$$

$$\lim_{(x-vt)\to-\infty} w_\mathrm{l}(x,t) < \infty, \qquad \lim_{(x-vt)\to\infty} w_\mathrm{r}(x,t) < \infty. \tag{4}$$

As the system is infinite and only locally inhomogeneous, the response is assumed to be in the steady state before the load reaches the transition zone. Consequently, initial conditions do not need to be formulated. Thus, Eqs. (1)–(4) constitute a complete description of the current problem.

The response of the inhomogeneous system described by Eqs. (1)–(4) can be obtained semi-analytically in various ways (e.g., [20]), but has not been determined fully analytically yet. We choose to apply the Fourier transform over time and represent the response as a summation of wave modes because we consider this method to be most elegant for this problem. The response obtained in the Fourier domain is analytical and the inverse transform is then performed numerically. The equation of motion in the Fourier domain reads

$$\tilde{w}'''' + k^4(x)\tilde{w} = -\frac{F_0}{EIv}\mathrm{e}^{-\mathrm{i}\omega\frac{x}{v}}, \tag{5}$$

$$k(x) = \begin{cases} k_\mathrm{l} = \sqrt[4]{-\overline{\rho}\omega^2 + \overline{k}_{\mathrm{d,l}}}, & x \le x_\mathrm{tc}, \\ k_\mathrm{r} = \sqrt[4]{-\overline{\rho}\omega^2 + \overline{k}_{\mathrm{d,r}}}, & x \ge x_\mathrm{tc}, \end{cases} \tag{6}$$

where the tilde denotes the quantity in the Fourier domain, the overbar indicates that the quantity is scaled by EI, and $\omega \in (-\infty,\infty)$ is the Fourier-domain variable. To determine $\tilde{w}$ from Eq. (5), a particular solution is superimposed to the solution of the homogeneous equation. The particular solutions $\tilde{w}_{p,l}$ and $\tilde{w}_{p,r}$ are sought for having the same spatial distribution as the forcing and read

$$\tilde{w}_{\mathrm{p,l}}(x,\omega) = -\frac{F_0}{EI}\frac{v^3}{\omega^4 - k_\mathrm{l}^4 v^4}\mathrm{e}^{-\mathrm{i}\omega\frac{x}{v}}, \qquad x \le x_\mathrm{tc}, \tag{7}$$

$$\tilde{w}_{\mathrm{p,r}}(x,\omega) = -\frac{F_0}{EI}\frac{v^3}{\omega^4 - k_\mathrm{r}^4 v^4}\mathrm{e}^{-\mathrm{i}\omega\frac{x}{v}}, \qquad x \ge x_\mathrm{tc}. \tag{8}$$

The particular solution $\tilde{w}_{p,l}$ is the frequency-domain eigenfield of a homogeneous system with the properties of the left domain (and analogously for $\tilde{w}_{p,r}$). In other words, evaluating the inverse Fourier transform of the particular solution would lead to the eigenfield. The complete solutions to Eq. (5) (including the solutions of the homogeneous equation) are given as follows:

$$\tilde{w}_\mathrm{l}(x,\omega) = A_\mathrm{l}\mathrm{e}^{-\mathrm{i}k_\mathrm{l}x} + B_\mathrm{l}\mathrm{e}^{\mathrm{i}k_\mathrm{l}x} + C_\mathrm{l}\mathrm{e}^{k_\mathrm{l}x} + D_\mathrm{l}\mathrm{e}^{-k_\mathrm{l}x} + \tilde{w}_{\mathrm{p,l}}(x,\omega), \qquad x \le x_\mathrm{tc}, \tag{9}$$

$$\tilde{w}_\mathrm{r}(x,\omega) = A_\mathrm{r}\mathrm{e}^{-\mathrm{i}k_\mathrm{r}x} + B_\mathrm{r}\mathrm{e}^{\mathrm{i}k_\mathrm{r}x} + C_\mathrm{r}\mathrm{e}^{k_\mathrm{r}x} + D_\mathrm{r}\mathrm{e}^{-k_\mathrm{r}x} + \tilde{w}_{\mathrm{p,r}}(x,\omega), \qquad x \ge x_\mathrm{tc}. \tag{10}$$

The four branches of k_h (where $h = \{l, r\}$) are all complex valued when ω is below the cut-off frequency $\omega_{co,h} = \sqrt{k_d/\rho}$ and when $\omega > \omega_{co,h}$, there are two real-valued and two imaginary-valued branches. The branches of k_h are chosen such that the imaginary part is negative and the real part is positive. This choice leads to $A_l = D_l = B_r = C_r = 0$ when the boundary conditions imposing a finite displacement at infinite distance from the load are applied, leading to the following expression for the displacement:

$$\tilde{w}(x,\omega) = \begin{cases} B_\mathrm{l} \mathrm{e}^{\mathrm{i}k_\mathrm{l}x} + C_\mathrm{l} \mathrm{e}^{k_\mathrm{l}x} + \tilde{w}_{\mathrm{p,l}}(x,\omega), & x \le x_\mathrm{tc}, \\ A_\mathrm{r} \mathrm{e}^{-\mathrm{i}k_\mathrm{r}x} + D_\mathrm{r} \mathrm{e}^{-k_\mathrm{r}x} + \tilde{w}_{\mathrm{p,r}}(x,\omega), & x \ge x_\mathrm{tc}. \end{cases} \tag{11}$$

The remaining four amplitudes are determined from the interface conditions (Eqs. (2) and (3)). Their expressions are not given here for brevity, but can be obtained straightforwardly by using a symbolic mathematical software (e.g., Maple or Mathematica). To obtain the solution in the time domain, the inverse Fourier transform is applied numerically.

RESULTS

Response amplification at transition zones

Fig. 2 presents the transient response in the time domain together with the eigenfield (of an homogeneous system with the properties of the left domain) for comparison. Far away from the transition zone, the two responses are practically identical (theoretically they are identical only at $t \to -\infty$). When the moving load is close to the transition, the transient response is distorted in comparison to the eigenfield. In the process of the load passing the transition, waves are radiated; the most noticeable are propagating in negative *x*-direction, although the wave radiation occurs in both directions. Furthermore, evanescent waves that remain in the vicinity of the transition zone are also excited. It can also be observed that the wave propagation still occurs even when the load has left the transition zone (provided that the damping in the system is small).

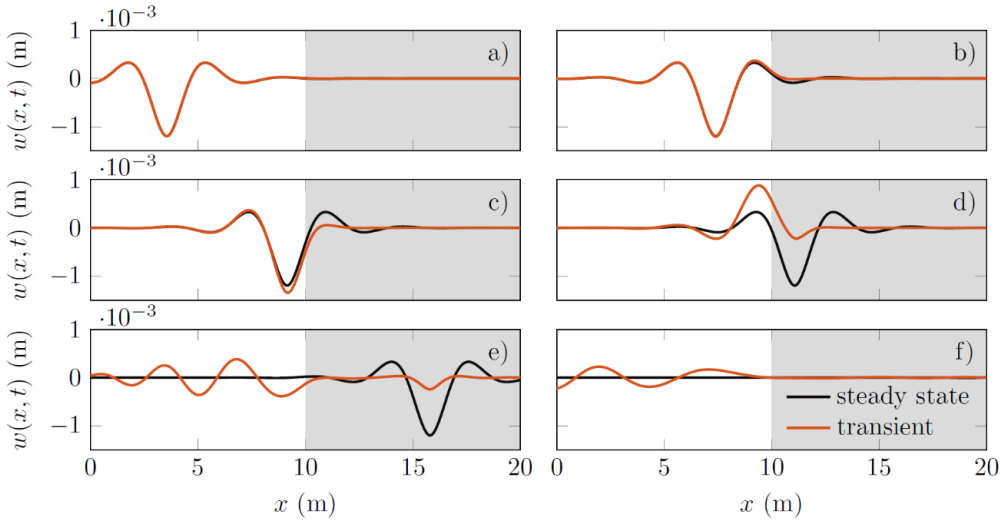

Figure 2: Snapshots of the displacement field at different time moments for the soft-to-stiff transition at a velocity of $v = 0.9c_{cr}$, where c_{cr} is the critical velocity. The stiff domain is represented through the grey background.

For certain time moments, amplification of the response can be observed in the vicinity of the load, both downwards and upwards (e.g., the two middle panels in Fig. 2). This is the amplification of stresses and strains that can be associated with the differential settlements at transition zones [7] (although Fig. 2 presents displacements, the force in the foundation is obtained when multiplying the displacement by $k_d(x)$). The response amplification is caused by the interference of the incoming eigenfield and the reflected wave-field at the transition, referred to as the *free field*. Mathematically, the free field is nothing else than the homogeneous solution (see Eq. (11)) that is necessary to satisfy the interface conditions. It becomes obvious that the more pronounced the free field is compared to the eigenfield, the larger the amplification (the amplification is always relative to the approaching eigenfield).

Soft-to-stiff vs stiff-to-soft transition types

Fig. 3 presents a comparison of the two transition scenarios. The displacement evaluated under the moving load is presented for a relatively low velocity $v = 0.5c_{cr}$ (top panels) and a relatively high velocity $v = 0.95c_{cr}$ (bottom panels), where c_{cr} is the critical velocity. To highlight the response amplification, the steady-state displacement under the moving load (corresponding to the soft domain) is also presented through the horizontal dashed lines. Note that only the one in the soft domain is presented because we are interested in the response amplification before (for the soft-to-stiff) and after (for the stiff-to-soft) the man-made structure. The reason for this is that most of the differential settlement occurs in the zones adjacent to the man-made structure, and not on it [15].

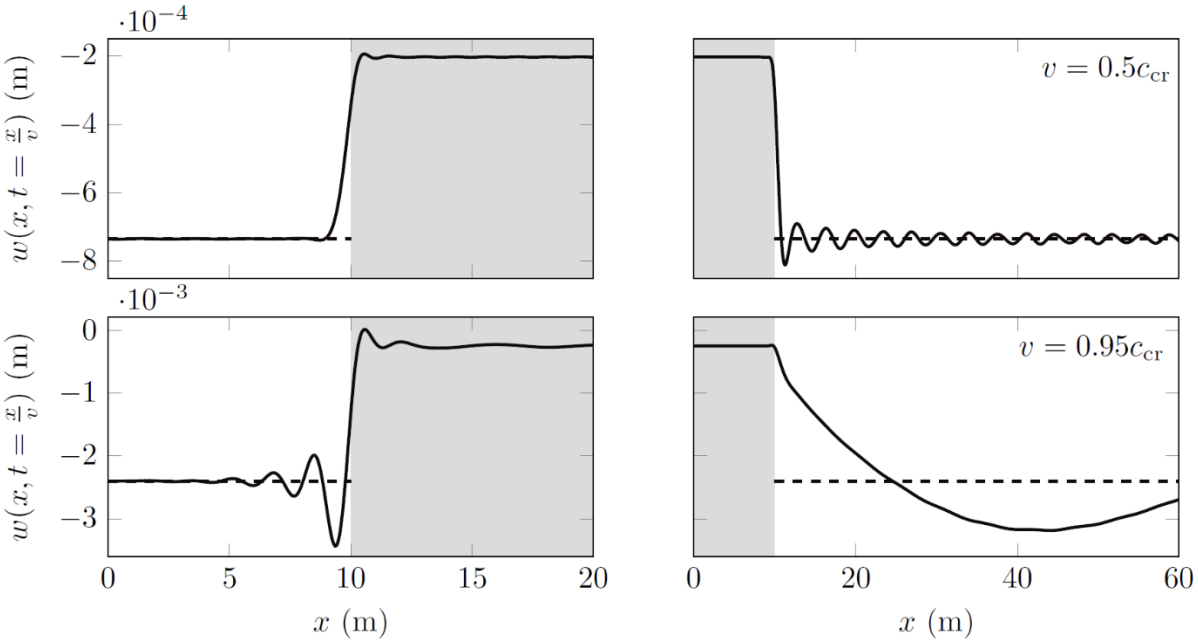

Figure 3: The transient response evaluated under the moving load in the soft-to-stiff scenario (left panels) and stiff-to-soft one (right panels) for a relatively low velocity v = 0.5c_{cr} (top panels) and a relatively high velocity v = 0.95c_{cr} (bottom panels); c_{cr} is the critical velocity. The stiff domain is represented through the grey background, while the horizontal dashed lines indicate the steady- state displacement in the soft domain evaluated under the moving load.

Fig. 3 shows that for a relatively small load velocity, the results in the two scenarios are similar, even though the amplification in the stiff-to-soft scenario is slightly larger than in the soft-to-stiff one. More importantly, the amplification in both scenarios for the small velocity (top panels) is significantly lower compared to the large velocity (bottom panels). For the large velocity, the responses in the two scenarios are significantly different. In the soft-to-stiff scenario, the eigenfield travelling in positive x-direction interferes with the free-field travelling in negative x-direction, leading to the response under the moving load to oscillate with a high frequency. In the stiff-to-soft scenario, both interfering fields (eigenfield and free field) travel in positive x-direction, and for the large speed ($v = 0.95c_{cr}$), they have similar travelling velocities. This leads to their constructive interference to occur over a much larger distance, and to a low frequency oscillation of the response under the moving load. This implies that, for a relatively large velocity, the settlement in the soft-to-stiff scenario will occur close to the stiff zone and will have a small wavelength, while the opposite is true for the stiff-to-soft scenario.

Fig. 3 also shows that the maximum response amplification in both transition types is similar in magnitude. However, this is only the case for the system without material damping. Once damping is accounted for in the foundation, the free field decays with distance from the transition. This causes the amplification in the stiff-to-soft scenario, which occurs at a large distance from the transition, to decrease considerably even when prescribing a small amount of damping. This is shown in Fig. 4 that presents the maximum amplification in both scenarios versus relative load velocity (v/c_{cr}), for a small (top panel) and a large (bottom panel) amount of damping. The addition of damping causes the maximum amplification in the stiff-to-soft case to decrease at large relative velocities to values even smaller than at low relative velocities, while the presence or amount of damping does not significantly influence the amplification trend in the soft-to-stiff case (it does affect the magnitude, but not the trend). It is important to note that, at low to medium relative velocities, the maximum amplification in the stiff-to-soft scenario can be larger than in the soft-to-stiff one, but the velocity range over which this occurs decreases the higher the damping is.

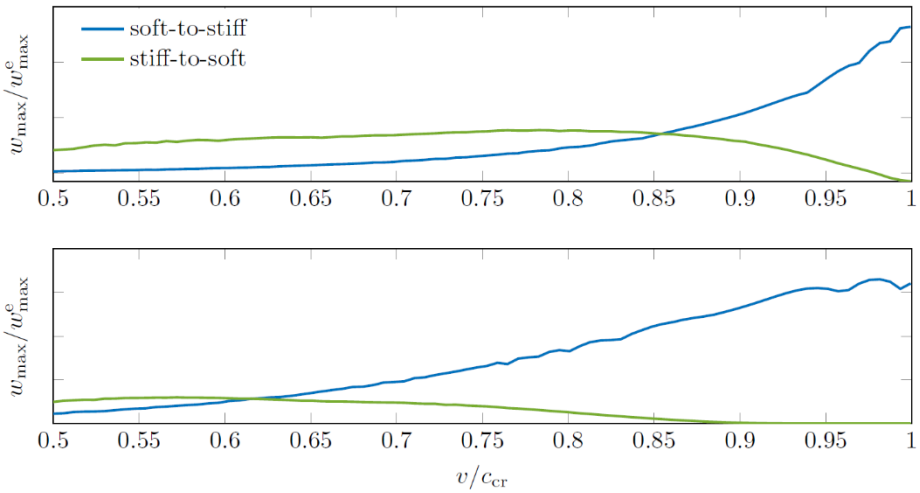

Figure 4: The maximum amplification (i.e., maximum transient response w_{max} relative to the maximum steady-state response w^e_{max}) versus velocity of the moving load for a small amount (top panel) and a large amount (bottom panel) of foundation damping for both soft-to-stiff and stiff-to- soft scenarios.

DISCUSSION

The low-fidelity model used in this study enables the exploration of wave-field interference that leads to the response amplification asymmetry observed in the previous section. However, it omits several factors that could potentially influence the transition process and the associated response amplification, such as a more detailed vehicle model (e.g., multiple wheels and the vehicle's own degrees of freedom), precise modeling of the substructure with layers of varying properties, the inclusion of wave propagation in transverse directions (i.e., considering the three-dimensional nature of the problem), among others. While these factors may quantitatively affect the results, the wave-field interference that causes response amplification asymmetry is a fundamental aspect of the transition problem and will persist even when all these additional elements are incorporated. The extent to which this mechanism influences response amplification when the aforementioned factors are included remains to be explored in future research.

From a practical standpoint, the findings of this study reveal that the response amplification in the two transitions types show a fundamentally different behaviour. Therefore, it is crucial for researchers and engineers to consider both transition types when assessing transition zone performance. Moreover, these results indicate that effective mitigation measures should be specifically tailored for each type of transition to ensure efficiency.

CONCLUSIONS

This study compared the response amplification at railway transition zones for two transition types: soft-to-stiff and stiff-to-soft. The goal was to explain the difference observed in differential settlement between the two transition types, both observed in field measurements (e.g., [15]) and in numerical simulations (e.g., [16]). To this end, a simplified model of a railway track with a transition zone was formulated; more specifically, the model consists of an Euler–Bernoulli beam resting on a Winkler foundation with a piecewise-homogeneous stiffness in space, acted upon by a moving constant load.

Although the soft-to-stiff and stiff-to-soft transitions seem to poses a certain symmetry, results show that their responses are quite distinct. It was shown that the response amplification at transition zones is caused by the interference between the steady-state field (eigenfield) and the free field generated during the transition process. Results show that the difference between the two transition types stems from the interference between the two wave-fields:

- In the soft-to-stiff scenario, the eigenfield travelling in positive *x*-direction interferes with the free-field travelling in negative *x*-direction, leading to the response under the moving load to oscillate with a high frequency.
- In the stiff-to-soft scenario, both interfering fields (eigenfield and free field) travel in positive *x*-direction, and for the large speed ($v = 0.95c_{cr}$), they have similar travelling velocities. This leads to their constructive interference to occur over a much larger distance, and to a low frequency oscillation of the response under the moving load.

Furthermore, the soft-to-stiff transition, the response amplification has been observed to be significant at load velocities between 75% and 100% of the critical one, and it increases considerably as the load velocity approaches the critical one. For the stiff-to-soft transition, the strongest response amplification occurs at lower velocities than for the soft-to-stiff ones, namely

between 50% and 80% of the critical velocity, after which the amplification decreases. These results strongly suggests that for a mitigation measure to be efficient, it should be designed differently for the two types of transition.

ACKNOWLEDGMENTS

This research is supported by the Dutch Technology Foundation TTW (Project 15968), part of the Netherlands Organisation for Scientific Research (NWO), and which is partly funded by the Ministry of Economic Affairs of the Netherlands.

REFERENCES

[1] P. Meijers, P. Holscher, and J. Brinkman. Lasting flat roads and railways: Literature study of knowledge and experience of transition zones. Technical report, GeoDelft, Delft, Netherlands, 2007.
[2] A. I. Vesnitskii and A. V. Metrikin. Transition radiation in one-dimensional elastic systems. *Prikladnaya Mekhanika i Tekhnicheskaka Fizika*, No. 2:62–67, 1992.
[3] A. I. Vesnitskii and A. V. Metrikin. Transition radiation in mechanics. *Physics-Uspekhi*, 39(10):983–1007, 1996.
[4] Karel N. van Dalen and Andrei V. Metrikine. Transition radiation of elastic waves at the interface of two elastic half-planes. *Journal of Sound and Vibration*, 310(3):702–717, 2008.
[5] Yao Shan, Bettina Albers, and Stavros A. Savidis. Influence of different transition zones on the dynamic response of track-subgrade systems. *Computers and Geotechnics*, 48:21–28, 2013.
[6] Karel N. van Dalen, Apostolos Tsouvalas, Andrei V. Metrikine, and Jeroen S. Hoving. Transition radiation excited by a surface load that moves over the interface of two elastic layers. *International Journal of Solids and Structures*, 73-74:99–112, 2015.
[7] Michael J. M. M. Steenbergen. Physics of railroad degradation: The role of a varying dynamic stiffness and transition radiation processes. *Computers and Structures*, 124:102–111, 2013.
[8] Andrei B. Fărăgău, Andrei V. Metrikine, and Karel N. van Dalen. Transition radiation in a piecewise-linear and infinite one-dimensional structure—A Laplace transform method. *Nonlinear Dynamics*, 98:2435–2461, 2019.
[9] Andrei B. Fărăgău, Traian Mazilu, Andrei V. Metrikine, Tao Lu, and Karel N. van Dalen. Transition radiation in an infinite one-dimensional structure interacting with a moving oscillator—The Green's function method. *Journal of Sound and Vibration*, 492, 2021.
[10] Andre Paixao, Jose Nuno Varandas, Eduardo Fortunato. Dynamic Behavior in Transition Zones and Long-Term Railway Track Performance. *Frontiers in Built Environment*, 7:1–16, 2021.
[11] Andrei B. Fărăgău, Joao M. de Oliveira Barbosa, Andrei V. Metrikine, and Karel N. van Dalen. Dynamic amplification in a periodic structure with a transition zone subject to a moving load: Three different phenomena. *Mathematics and Mechanics of Solids*, 27(9):1740-1760, 2022.

[12] Joao Manuel de Oliveira Barbosa, Andrei B. Fărăgău, Karel N. van Dalen, and Michael Steenbergen. Modelling ballast via a non-linear lattice to assess its compaction behaviour at railway transition zones. *Journal of Sound and Vibration*, 530:116942, 2022.
[13] Avni Jain, Andrei V. Metrikine, Michael J. M. M. Steenbergen, and Karel N. van Dalen. Dynamic amplifications in railway transition zones: Performance evaluation of sleeper configurations using energy criterion. *Frontiers in Built Environment*, 10:1285131, 2024.
[14] Jens C.O. Nielsen, Eric G. Berggren, Anders Hammar, Fredrik Jansson, and Rikard Bolmsvik. Degradation of railway track geometry—Correlation between track stiffness gradient and differential settlement. *Proceedings of the Institution of Mechanical Engineers, Part F: Journal of Rail and Rapid Transit*, 234(1):108–119, 2020.
[15] Bruno Zuada Coelho, Paul Holscher, Jeffrey Priest, W. Powrie, and F. Barends. An assessment of transition zone performance. *Proceedings of the Institution of Mechanical Engineers, Part F: Journal of Rail and Rapid Transit*, 225(2):129–139, 2011.
[16] Jose N. Varandas, Paul Holscher, and Manuel A.G. Silva. Settlement of ballasted track under traffic loading: Application to transition zones. *Proceedings of the Institution of Mechanical Engineers, Part F: Journal of Rail and Rapid Transit*, 228(3):242–259, 2014.
[17] Bruno Zuada Coelho, Jeffrey Priest, and Paul Holscher. Dynamic behaviour of transition zones in soft soils during regular train traffic. *Proceedings of the Institution of Mechanical Engineers, Part F: Journal of Rail and Rapid Transit*, 232(3):645–662, 2018.
[18] Khosrow Asghari, Saeed Sotoudeh, and Jabbar Ali Zakeri. Numerical evaluation of approach slab influence on transition zone behavior in high-speed railway track. *Transportation Geotechnics*, 28:100519, 2021.
[19] Ilaria Grossoni, Samuel Hawksbee, Pedro Jorge, Yann Bezin, and Hugo Magalhaes. Prediction of track settlement at high-speed railway transitions between embankment and bridge in the proximity of a turnout. *Transportation Geotechnics*, 37:100879, 2022.
[20] Andrei B. Fărăgău. Understanding degradation mechanisms at railway transition zones using phenomenological models. PhD thesis, Delft University of Technology, 2023.